To appear in
International Journal of Flow Control

Computational Study of the Effect of Slot Orientation on Synthetic Jet-Based Separation Control

Shawn Aram[1] and Rajat Mittal[2]

Department of Mechanical Engineering,
Johns Hopkins University, Baltimore, MD-21218

Abstract

A computational study is conducted to explore the effect of synthetic jet orientation on boundary layer separation control. A six-to-one aspect-ratio rectangular slot is chosen in the current study and streamwise and spanwise orientations of this slot are analyzed. In the first part of this study, the interaction of the jet with an attached laminar boundary layer for both slot configurations is examined. The dominant feature in the streamwise oriented slot is a pair of strong counter-rotating streamwise vortices and these are missing in the spanwise oriented slot configuration. These streamwise vortices undergo stretching and tilting to form a series of hairpin vortex structures and analysis shows that "sweeping" motions associated with these vortices bring high momentum fluid into the boundary layer. A variety of flow statistics are computed and these indicate that despite the smaller overall blockage represented by the streamwise oriented slot, it is more effective in increasing the momentum of the boundary layer. In the second part of this study, the slot orientation effect is examined for a separated flow over a wall-mounted hump at a chord Reynolds number of 1.5×10^4 at different operational conditions. Flow structures generated by the synthetic jet in both slot configurations in this case are similar to those in the case of attached boundary layer. A comparison of various instantaneous quantities which characterize the separation bubble size shows that the streamwise oriented slot achieves better performance for all jet velocities and most forcing frequencies in the range studied here. It is also found that the most effective frequency for both slot configurations is the one that matches with the dominant frequency of the baseline flow.

Nomenclature

A	=	cross sectional area of the slot, m^2
A_{sep}	=	area of reversed flow layer in the time-span averaged separation bubble zone, m^2
C_f	=	friction coefficient, $C_f = \tau_w / 0.5\rho U_\infty^2$
$\overline{C}_f$	=	time-span averaged of C_f
C_p	=	pressure coefficient, $C_p = (p - p_{ref}) / 0.5\rho U_\infty^2$
$\overline{C}_p$	=	time-span averaged of C_p
C_{uu}	=	streamwise momentum flux, N
c	=	chord length of the hump, m
d	=	slot width, m
F^+	=	nondimensional forcing frequency, $F^+ = fc/U_\infty$
f	=	frequency, 1/sec

[1] Current affiliation: U.S. Army Research Laboratory, Aberdeen Prooving Grounds, earam1@jhu.edu.
[2] Professor, Department of Mechanical Engineering, mittal@jhu.edu.

H = maximum height of the hump, m
h = slot height, m
L = spanwise space between geometric center of adjacent slots, m
L_{sep} = separation bubble length, m
L_z = span size of the computational domain, m
L_{sep_Sp} = separation bubble length in the spanwise oriented slot case, m
L_{sep_St} = separation bubble length in the streamwise oriented slot case, m
l = slot length, m
M = Mach number
p = static pressure, Pa
p_{ref} = reference pressure, Pa
Q = swirl strength, 1/sec
Re_c = chord Reynolds number, $Re_c = U_\infty c/\nu$
Re_J = jet Reynolds number, $\mathrm{Re}_J = \overline{V}_J d/\nu$
Re_δ = boundary layer Reynolds number, $Re_\delta = U_\infty \delta/\nu$
S = Stokes number, $S = \sqrt{2\pi f d^2/\nu}$
St = Strouhal number, $St = S^2/Re_J$
T = period of excitation, sec
t = time, sec
U_∞ = free-stream velocity, m/sec
u = streamwise velocity, m/sec
u' = fluctuation velocity in streamwise direction, m/sec
$|\overline{u'v'}|$ = time-span average of $u'v'$, m^2/sec^2
$\overline{V}_J$ = time-space average of jet exit velocity during the expulsion phase, m/sec
v_J = jet exit velocity, m/sec
v = cross-stream velocity, m/sec
v' = fluctuation velocity in cross-stream direction, m/sec
x_{sep} = location of the boundary layer separation, m
x_{re} = location of the boundary layer reattachment, m
x = streamwise coordinate
y_0 = height of the reverse flow layer, m
y = cross-stream coordinate
z = spanwise coordinate
δ = boundary layer thickness, m
ν = kinematic viscosity, m^2/sec
ρ = fluid density, kg/m^3 ϕ = phase of excitation, degree
ζ = vorticity, 1/sec
Ω = vorticity flux, m^3/sec^2
τ_w = span averaged wall shear stress, N/m^2

1. INTRODUCTION

Modification of a flow field with an aim of advancing aerodynamic efficiency and performance has been of interest to aerodynamicists at least as far back as the discovery of the boundary layer by Prandtl [1]. In general, boundary layer modification can be achieved by preventing/provoking separation, delaying/advancing transitions, suppressing/enhancing turbulence, which may lead to drag reduction, lift enhancement, noise suppression, mixing augmentation, etc [2]. Among several separation control techniques, zero-net mass-flux (ZNMF) or synthetic jet actuators have emerged as highly useful and effective actuators. These actuators are suitable for both open-loop and closed-loop flow control techniques. Apart from active separation control, ZNMF actuators have many other applications including heat transfer [3], mass transfer [4], thrust vectoring [5, 6], mixing enhancement

[7, 8], vibration [9] and noise suppression. However, since the current study is motivated by separation control, we focus primarily on synthetic jets in cross-flow.

Because of versatility of these actuators, many numerical and experimental studies have been conducted to identify the performance characteristics, flow physics, and control effectiveness of these devices in cross-flow boundary layers. Since the operational parameters such as jet velocity, frequency and duty cycle can be modified on demand (in a feed-forward or feedback mode) for a given actuator, most of the past studies have focused on these parameters and their effect on the jet-cross-flow interaction. These include the studies of Crook & Wood [10], Mittal *et al*. [11], Mittal & Rampunggoon [12], Zhong *et al.* [13], Jabbal & Zhong [14], Schaeffler & Jenkins [15], Gorden & Soria [16], Wu & Leschziner [17], Dandois *et al*. [18] and Zhou & Zhong [19]. Of particular note here is the experimental study of Zhong *et al.* [13] who studied the effects of Reynolds number, Strouhal number and velocity-ratio on the vortical structures produced by circular synthetic jets in a laminar boundary layer. Stretched hairpin vortices which attached to the wall were generated by the synthetic jet at low Reynolds numbers and velocity-ratios. It was hypothesized that the streamwise vortices produced by these hairpin structures could be desirable for separation control. Roll-up of jets into vortex ring followed by tilting and stretching occurred at an intermediate Reynolds number and velocity ratio. By increasing these two flow parameters, rapid penetration of the tilted vortex ring up to the edge of the boundary layer with very slight effects on the flow close to the wall was observed. Jabbal & Zhong [14] performed a similar study of a circular synthetic jet in a laminar boundary layer and showed that the stretched vortex rings with a longitudinal vortex pair embedded in the boundary layer produced the highest net improvement and streamwise persistence of the wall shear stress in comparison with the hairpin and tilted vortical structures and as a result could provide most effective flow separation control.

A recent study of note is that of Vasile *et al.* [20] who investigated the interaction of a finite-span synthetic jet with the rectangular jet slot of aspect-ratio 27 on the flow over a swept NACA 4421 airfoil for two different jet velocities. The chord length based Reynolds number of the flow was 10^5 and the airfoil was held at a zero angle-of-attack. The PIV measurements of the flow showed the presence of streamwise structures due to the finite-span of the jet, and spanwise structures produced by the vortex pair emanating from the slot. Highly three dimensional flow in the vicinity of the orifice due to the edge effects and immediate breakdown of vortical structures were observed in this study.

In contrast to these operational parameters, the shape and orientation of the jet slot is essentially fixed once the actuator is emplaced in the flow. While these features do not affect the instantaneous mass flux from the jet (assuming that the jet slot area is kept constant), they can potentially have a significant effect on the momentum and vorticity fluxes from the jet. This in turn can significantly modify the impact of the synthetic jet on the cross-flow boundary layer [11, 12]. Thus, the jet slot geometry and orientation needs to be chosen carefully in order to ensure the highest level of the control effectiveness for a given actuator. However, despite this, relatively little attention has been paid to these features. This is likely due to a number of factors: first, changing the jet shape and orientation requires significant effort both in experiments and numerical studies with the former requiring physical changes to the jet and the latter, changes to the computational mesh. Second, while changes in these features might modify the jet boundary layer interaction, extracting fundamental insights into underlying flow mechanisms that can be extended beyond specific configurations/applications is difficult since the effects are usually highly three-dimensional.

Notwithstanding these difficulties, there have been a few notable studies that have examined jet shape and orientation effects. First among these is the experimental study of Smith [21] who examined the interaction between a synthetic jet array and a cross-flow turbulent boundary layer for streamwise as well as spanwise orientations of a rectangular jet slot. The jet slot had an aspect-ratio of 45 and a spanwise orientation of the slots was found to provide a significant blockage in the near flow field. For a streamwise oriented slot configuration, the formation of longitudinal vortices in the boundary layer caused sweeping of the high momentum fluid toward the wall along the jet centerline and away from the wall in the off-center regions. A higher penetration of the jet into the boundary layer was also observed in the streamwise oriented slot case. However, a full understanding of the 3D flow structures was limited due to the hot-wire anemometry technique that was employed in this study. The experiments of Milanobic & Zaman [22] examined the effect of the jet pitch and yaw on a cross-flow

and showed that increasing the pitch angle with respect to the surface caused a higher penetration of the jet, whereas increasing the yaw angles led to enhanced jet spreading. They also found that the streamwise velocity inside the jet-vortex structure depended on the momentum-flux ratio.

Thus it seems that the jet orientation has the potential of significantly altering the effect of the synthetic jet on the external cross-flow. However, unlike other jet operational parameters like frequency and amplitude, which can be changed to optimize the performance of the actuator for a certain flow condition, the jet slot orientation can not be changed once the actuator is designed and installed. Therefore, a careful choice of this feature could significantly enhance the control authority of a given actuator. Motivated by this, we examine the effect of synthetic jet orientation on an attached laminar boundary layer over a flat plate using numerical simulations with the aim of understanding the fundamental flow physics that could explain this effect. Using this knowledge and based on the fact that the past studies have not investigated this effect on a separated flow, we examine the relative effectiveness of the actuator in two different orientations on the separated flow downstream of a wall-mounted hump. This geometry, which is one of the test cases considered in the 2004 NASA Workshop on the synthetic jet validation, was first proposed by Seifert and Pack [23] to study turbulent flow separation and control at high Reynolds numbers ($O(10^6)$). They conducted a series of experiments using a cryogenic tunnel for the baseline and controlled cases (by means of steady suction/blowing and periodic excitation) and provided a comprehensive database for the CFD validation. In addition to the CFD studies of the flow over a hump which were presented in the NASA Workshop 2004 and are summarized by Rumsey *et al*. [24], some other ZNMF based separation control studies of this flow configuration are by You and Moin [25], Saric et al. [26], Rumsey [27], Bettini & Cravero [28], and Franck and Colonius [29]. It needs to be pointed out that in all of these studies, the jet slot extended across the entire length of the span.

Two different slot configurations with respect to the cross-flow are studied in the present work; both configurations have rectangular jets slots arranged in a spanwise periodic array; however in one configuration, the long axis of the slot is oriented in the spanwise direction whereas in the other, it is oriented in the streamwise direction. In both configurations we consider a spanwise periodic array of slots in a cross-flow. The performance of the ZNMF actuator for different operational conditions (amplitude and frequency) for both slot configurations is also investigated for the case of separated flow.

This paper is organized as follows: Section 2 provides a description of the computational setup including the flow configurations, boundary conditions, synthetic jet characteristics and the numerical methodology used to simulate the attached and separated flow. In Section 3, which consists of three parts, a discussion of the numerical results is given; in the first part of this section, a description and discussion of the results for the attached boundary layer case including the mean and instantaneous flow characteristics for both synthetic jet configurations is provided. In the second part, the baseline uncontrolled flow over a wall-mounted hump is validated with published results and some aerodynamic parameters are explored. The third past of this section describes the study of the effect of slot orientation on the flow over the hump at different jet amplitudes and frequencies.

2. FLOW CONFIGURATION

2.1 Slot Configurations in Cross-Flow

Figure 1(a) and 1(b) shows a top view (x-z plane) of the spanwise and streamwise oriented slot configurations in a cross-flow, respectively. The aspect ratio (length to width, l/d) of slots is chosen to be equal to six for both configurations and the spacing between the geometric centers of the adjacent slots (L) is 1.5 time of the slot length. The chosen aspect-ratio is such that while both cases are expected to show significant three-dimensional behavior associated with the end-effects, there should also be a noticeable difference between the two orientations. In order to limit the computational expense of these simulations, we only consider one synthetic jet and a spanwise domain of L in our simulations and the effect of adjacent actuators is imposed by applying a periodic boundary condition at the spanwise domain boundaries.

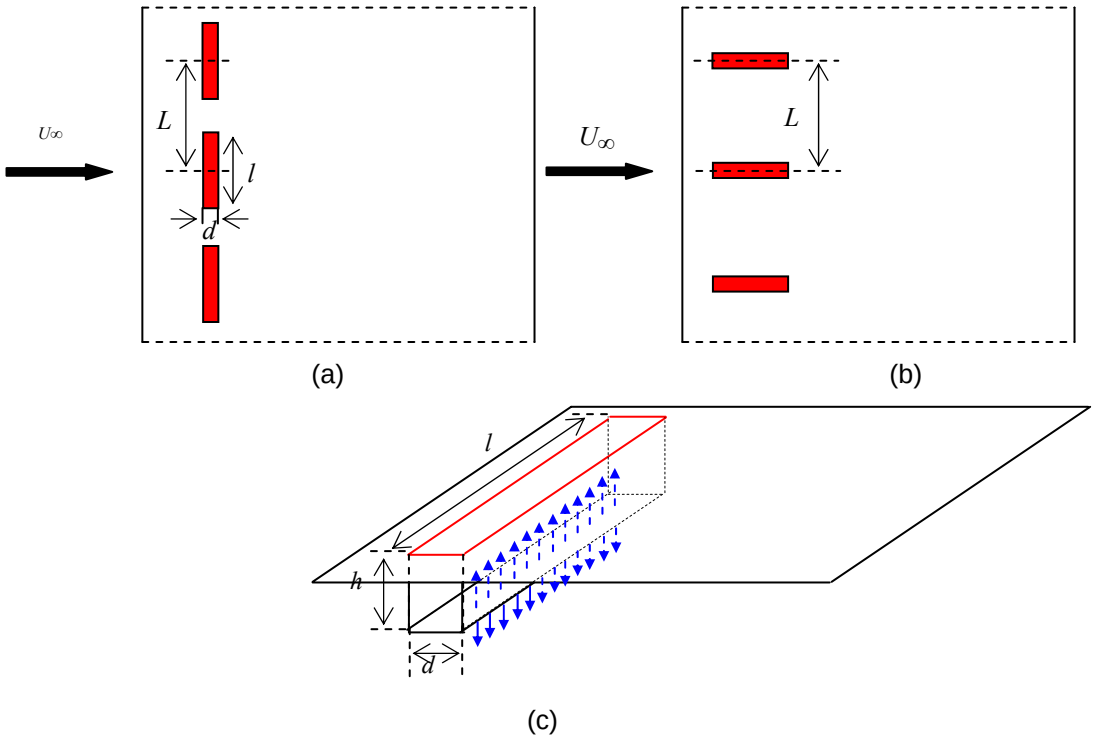

Figure 1. Array of (a) spanwise oriented slots, and (b) streamwise oriented slots, (c) 3D view of synthetic jet

Accurate representation of the jet emanating from the slot is an important aspect of these simulations. The presence of the cross-flow can significantly modify the jet velocity profile, which in turn changes the momentum, energy and vorticity flux from the jet [30, 31]. Consequently, inaccurate representations of the jet exit velocity profile (for instance by specifying some canonical velocity profile at the jet exit) can lead to results that do not correctly represent the true effect of the jet on the flow [30]. On the other hand, modeling the entire actuator including the cavity and slot can add significantly to the expense of these simulations. Our previous study [31] has shown that a model of the actuator which includes only the slot, is able to capture most of the flow physics associated with a jet in a cross-flow and produce a highly representative jet exit velocity profile. We therefore employ this "slot-only" model in the current simulations. Figure 1(c) shows the schematic of the 3D view of the synthetic jet in a cross-flow. The height-to-width (h/d) ratio of the slot is fixed to a value of one in all the simulations. A uniform, temporally sinusoidal vertical velocity condition is imposed at the bottom of the slot. The time-average of jet velocity over the expulsion phase is given by:

$$\overline{V}_J = \frac{2}{AT}\int_0^{T/2}\int_A v_J(x,t)\,dA\,dt \tag{1}$$

where, $v_J(x,t)$ is the vertical jet velocity along the jet exit plane, A is the cross sectional area of slot, and $T=1/f$ is the period of the synthetic jet actuator oscillations.

2.2 Attached Boundary Layer Configuration

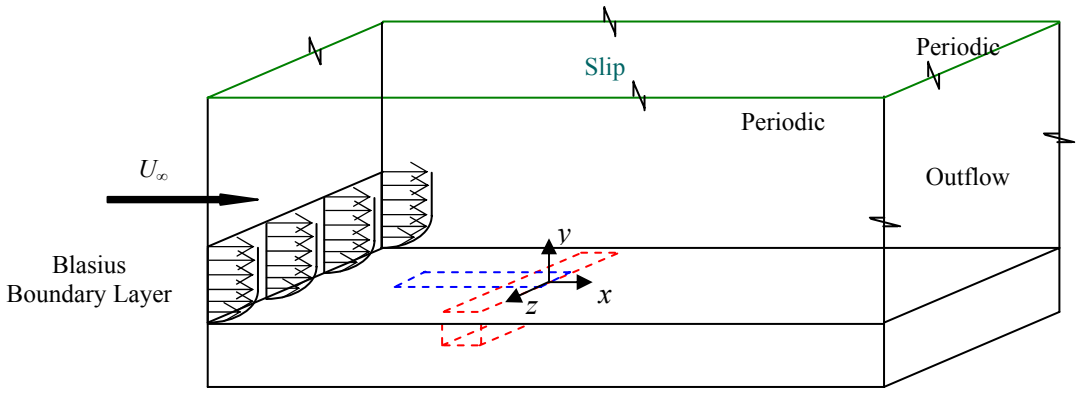

Figure 2. Computational domain of study for both synthetic jet configurations (not to scale)

Figure 2 shows the computational domain used to study the effect of jet orientation in an attached laminar cross-flow. The flow at the inlet located at the left side of the domain, is prescribed by a cubic approximation to the Blasius boundary layer over the flat surface. For a boundary layer thickness of δ and free-stream velocity U_∞, the velocity for $y<\delta$ is defined as:

$$\frac{u}{U_\infty}=\frac{3}{2}\frac{y}{\delta}-\frac{1}{2}\left(\frac{y}{\delta}\right)^3 \tag{2}$$

and for $y>\delta$, the velocity is equal to the free-stream velocity, U_∞. On the right side of the domain, an outflow boundary condition is prescribed which allows the vortex structures to convect out of the domain with minimal reflections. A no-slip condition is applied on the bottom wall and a slip-wall boundary condition is applied on the top boundary. The dimensionless flow parameters for the simulations are chosen as follows: $\delta/d=2$, $\overline{V_J}/U_\infty=0.25$, jet Reynolds number $\mathrm{Re}_J=\overline{V_J}d/\nu=150$ (which results in a boundary layer thickness based Reynolds number $\mathrm{Re}_\delta=U_\infty\delta/\nu=1200$) and a Stokes number $S=\sqrt{2\pi fd^2/\nu}=6.86$. While the Reynolds numbers are consistent with the laminar nature of the boundary layer being studied here, the values of δ/d and $\overline{V_J}/U_\infty$ are quite realistic [13, 14, 19] and have been chosen in past computational studies [30, 31, 32, 33]. It should be noted that the Strouhal number, defined as $2\pi fd/\overline{V_J}$ comes out to be 0.31 for these chosen parameters and this ensures the formation of robust vortices at the exit of the synthetic jet [34].

A second-order fractional-step method is used to solve the incompressible Navier-Stokes equations on Cartesian grids [35]. The solver employs a second-order Adams-Bashforth scheme for the convective terms and an implicit Crank-Nicolson scheme for the diffusion terms. A sharp-interface immersed boundary method is employed to incorporate the effect of all the solid boundaries body on the flow. The simulation is carried out on a domain with a size of $50d\times40d\times9d$ and a $256\times128\times96$ non-uniform grid is employed. The synthetic jet is located at $14d$ from the inlet boundary and the large domain size ensures that boundary effects do not significantly affect the computed flow in the vicinity as well as in the interaction region immediately downstream of the jet. A grid dependency study is conducted with a $256\times256\times128$ grid, where the total number of grid points in and around the synthetic jet is nearly doubled. Despite this significant increase in resolution, no noticeable differences in the flow and vorticity field are found [36] between the two simulations. Thus, the original resolution is deemed sufficient for the current simulations.

2.3 Separated Boundary Layer Configuration

Figure 3 shows a side view of the model geometry employed in the study of the effect of the slot orientation on a separated flow. This hump geometry is essentially the suction side of a Glauert-Goldschmied airfoil at zero angle of attack with some modifications, and is similar to the one that was first studied by Seifert and Pack [23] experimentally. Separation of the boundary layer occurs on the convex side of the body before the trailing edge and is followed by an unsteady turbulent separation bubble that extends downstream of the model.

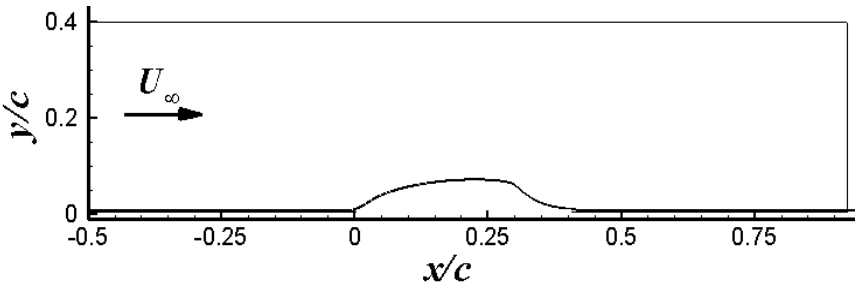

Figure 3. Geometry of wall-mounted hump

The computational domain and boundary conditions used for this geometry are given in Figure 4. The 1/7 power law turbulent velocity profile [37] with zero turbulence intensity is imposed on the left side of the domain within the boundary layer thickness δ and is defined as:

$$\frac{u}{U_\infty} = \left(\frac{y}{\delta}\right)^{1/7} \tag{3}$$

where the velocity outside the boundary layer is equal to the free-stream velocity, U_∞. Thus we model, in the mean, the effect of turbulence on the distribution of streamwise momentum in the boundary layer. On the right side of the domain, and outflow boundary condition is employed to convect vortex structures out of the domain with minimal reflections. A no-slip boundary condition is used for all walls and symmetry boundary condition (which is intended to match the BC of Franck [38]) is prescribed on the top boundary.

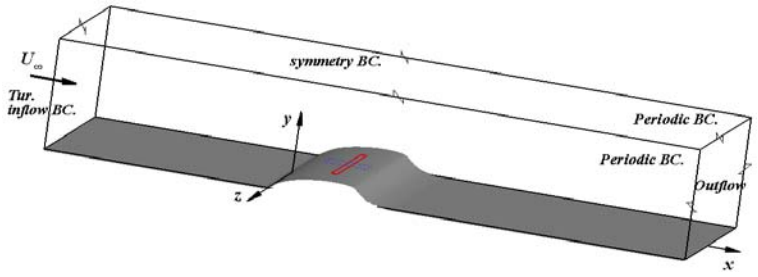

Figure 4. Computational domain employed in the simulations of flow over the wall-mounted hump; solid line: spanwise oriented slot, dashed line slot: streamwise oriented slot (not to scale)

Both synthetic jet configurations shown in Figure 4 are part of the array of synthetic jets that are located along the model span. These configurations are similar to the ones described in section 2.2. The geometric center of both slots is located at *x/c*=0.54 such that the right streamwise edge of both

slots is slightly upstream of separation point. Note that the leading and trailing edges of the hump are located at x/c=0 and x/c=1, respectively.

For this flow configuration we keep the external flow conditions as defined by Re_c and δ/d constant (1.5×10^4 and 8, respectively) and vary the two key parameters for this actuator which are $\overline{V_J}/U_\infty$ and the forcing frequency (F^+). The following values for these two parameters are used: $\overline{V_J}/U_\infty$ = 0.095, 0.254, 0.445 and F^+ = 1.87, 2.1, 4 and 8.

The flow solver that is used in this study is the same as the one used for the attached boundary layer configuration described in section 2.2. However, to accommodate flow transition and turbulence effects at the higher Reynolds number of this flow, we employ a large-eddy simulation (LES) approach. The LES model is based on the global dynamic coefficient subgrid-scale modeling approach introduced by Vreman [39] and further details of the implementation of this LES model in the solver can be found in [40]. A domain size of $4.4c\times0.909c\times0.09c$ has been chosen for this set of simulations and this is similar to the numerical study of Franck [38] in the x-y plane. This domain is large enough to ensure that the boundary effects on the computational results, especially in the separation zone are negligible. For all simulations, a dense 512×128×64 non-uniform grid is employed and a grid dependency study is carried out by applying finer grids in the separation region in streamwise (x) and wall-normal (y) directions, and a uniform grid in the spanwise (z) direction for the baseline flow. This grid dependency study is presented in section 3.2.1.

3. COMPUTATIONAL RESULTS

3.1 Jet Interaction with Attached Flat Plate Boundary Layer

In this section, the flow physics associated with the interaction of the synthetic jet with an attached laminar boundary layer for both slot configurations is discussed.

3.1.1 Instantaneous flow field

The magnitude of the imaginary part of the complex eigenvalue of the velocity gradient tensor (swirl strength: Q) is used here to identify three-dimensional vortex structures [41]. Figure 5 shows five snapshots of the instantaneous iso-surface of this quantity corresponding to a non-dimensional magnitude of $0.25Qd/U_\infty$, with contours of vertical velocity ($v/\overline{V_J}$) shown on the iso-surfaces. The figure compares the vortex structures for both cases at five different phases in the jet cycle. Note that $\phi = 90^\circ$ and $\phi = 270^\circ$ correspond to the maximum expulsion and maximum ingestion phases, respectively.

Figure 5A(i) and B(i) correspond to the middle of the expulsion cycle and the difference between the two jet orientations is readily apparent even at this early stage. For the spanwise oriented slot case, the primary feature is a spanwise oriented structure just downstream of the jet slot that extends across the span of the slot. Similar to what was found in the experimental study of Vasile *et al*. [20], there are small streamwise oriented vortices that emanate from the spanwise ends of the slot. In contrast, the dominant feature for the streamwise oriented slot case as seen in the experimental work of Smith [21], is a pair of counter rotating streamwise vortices that are attached to the spanwise ends of the slot and which form the legs of a large hairpin vortex. This clear difference is driven primarily by the fact that for the flow through the spanwise oriented slot, the streamwise gradient of the flow velocity (and hence the spanwise vorticity) scales as $\left(\overline{V_J}/d\right)$ and far exceeds the spanwise gradient (and the streamwise vorticity) which scales as $\left(\overline{V_J}/l\right)$, whereas the case is exactly the opposite for the streamwise oriented slot case. This is very clearly seen in the plots of vorticity along two orthogonal planes through the jet slot at this phase of the jet cycle (Figure 6). The figures also show that for the spanwise oriented slot case, the clockwise spanwise vorticity in the cross-flow boundary layer cancels out most of the vorticity in the spanwise vortex of the jet which has counterclockwise vorticity.

At a later phase corresponding to $\phi = 135^{\circ}$ shown in Figure 5A(ii) and B(ii), we observe a further amplification in the differences between the two cases. While there is some downstream growth in the streamwise components of the structures emanating out of the spanwise oriented slot, the hairpin vortex from the streamwise oriented slot has already spawned an additional hairpin head immediately upstream of the original structure. Furthermore, the original hairpin has grown considerably in size during this time and the mutual induction of streamwise vortices causes the lift-up of the head and legs of hairpin structures from the wall. At a later time corresponding to 6(iii), we find that the weaker streamwise vorticity from the spanwise oriented slot has also spawned a small hairpin-like structure whereas the hairpins from the streamwise oriented vortices have grown stronger and larger. At still later times, it is noted that the vortices from the streamwise oriented slot results in a conglomeration of vortices which occupy a larger extent in both the streamwise and wall-normal directions than the corresponding vortex structure of the spanwise oriented slot. As a consequence, the overall vertical penetration of the jet in the streamwise oriented slot case is greater than the spanwise oriented slot case and this is inline with the experimental study of Smith [21].

As observed in the experimental study of Acarlar & Smith [42] accumulation and lift-up of low momentum fluid between the counter rotating legs in the trailing region of hairpin vortices occurs due to lateral pressure gradients. They synthesized hairpin vortices in a laminar boundary layer by continuous injection through a thin streamwise slot. Downwash of fluid occurs outboard of counter rotating legs to replace the lifted up fluid between the hairpin legs (mass conservation) which leads to the formation of saddle points in either side of the hairpin structure and development of secondary streamwise vortices outboard of these saddle points with an opposite sense of rotation [43]. These secondary vortices seen in the tip of the hairpin structure in all the snapshots in the streamwise oriented slot (Figure 5B(i)-B(v)) might be responsible for the spanwise spreading of the jet as it convects downstream.

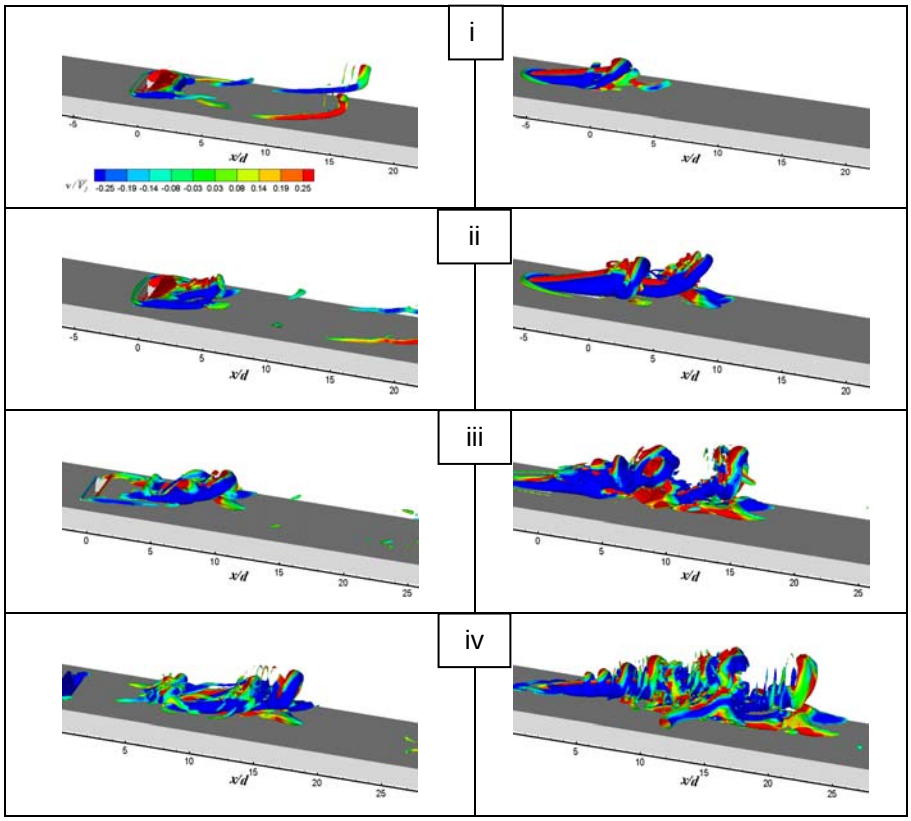

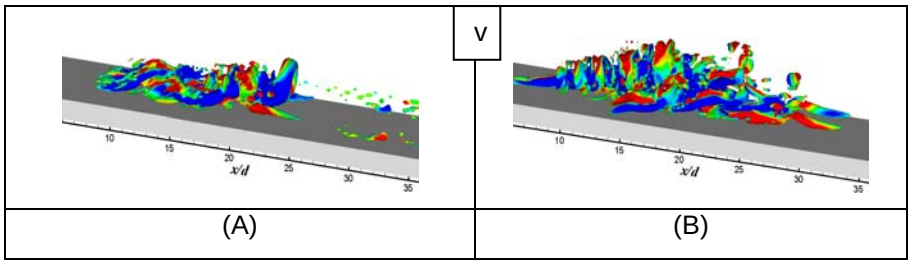

Figure 5. Instantaneous iso-surface of the swirl strength colored by the cross-stream velocity contours for the (A) spanwise orientated slot and (B) streamwise oriented slot at: (i) $\phi = 90^\circ$ (maximum expulsion phase), (ii) $\phi = 135^\circ$, (iii) $\phi = 180^\circ$, (iv) $\phi = 225^\circ$, (v) $\phi = 270^\circ$ (maximum ingestion phase)

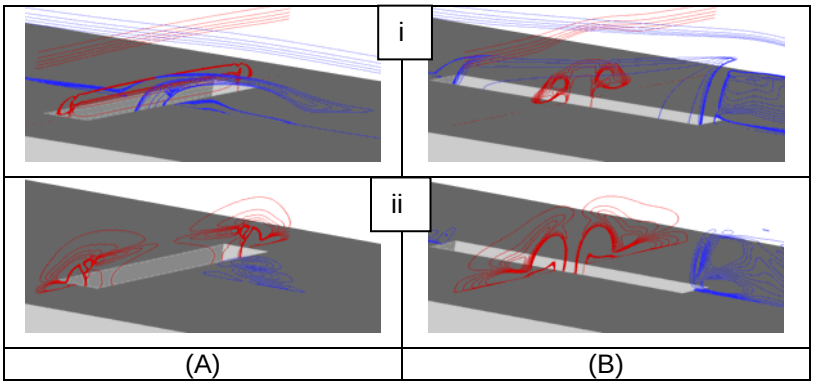

Figure 6. Contours of the (i) spanwise and (ii) streamwise vorticity on the *x-y* and *y-z* center-planes for the (A) spanwise oriented slot, (B) streamwise oriented slot

In order to understand the effect of the vortex structures on the boundary layer flow downstream of the slot, the phase averaged *u*-velocity profiles along the vertical direction (*y*) are extracted and examined. Figure 7 shows a comparison of these profiles for both slot orientations as well as the baseline, undisturbed flow. Note that in all of figures shown in this paper, "Sp" and "St" represents the spanwise and streamwise oriented slot cases, respectively. Since the flow is almost symmetric with respect to the centerline in the vicinity of slot, only the velocity profile in one half of the span is examined. Three phase instances between maximum expulsion and maximum ingestion phases and, three different spanwise locations (z/d=0 bottom row, z/d=-1.5 middle row, and z/d=-3 top row) at a fixed streamwise location of x/d=4 are chosen for this comparison. Each column in the figure represents one phase-instance. The streamwise velocity (u) and vertical (y) coordinate are normalized by the free-stream velocity and local boundary layer thickness of the unexcited flow, respectively. Figure 7(a) shows the velocity profile at the maximum expulsion phase ($\phi = 90^\circ$ which corresponds to Figure 5(i)) and we note that advection of the vortical structures causes a slight velocity deficit in the spanwise oriented slot case between $0.3<y/\delta<1.0$, with a small increase in the peak velocity.

Formation of hairpin structures and up-wash of the low-momentum fluid at the mid-span in the streamwise oriented slot case leads to significant slowing down of the flow in comparison with the baseline flow during the expulsion phase ($\phi = 90^\circ$ and $\phi = 180^\circ$). Although the velocity profile is almost unchanged away from the mid-span in this case at $\phi = 90^\circ$ due to the limited spreading of the jet along the spanwise direction. Downwash of high-momentum fluid by the secondary streamwise vortices outboard of hairpin legs are responsible for dramatic augmentation in the velocity near the surface at z/d=-1.5 and slight increase at z/d=-3 at $\phi = 180^\circ$. As expected, a velocity deficit is observed between $0.3<y/\delta<1.0$ at z/d=-1.5 at this phase to satisfy the mass conservation.

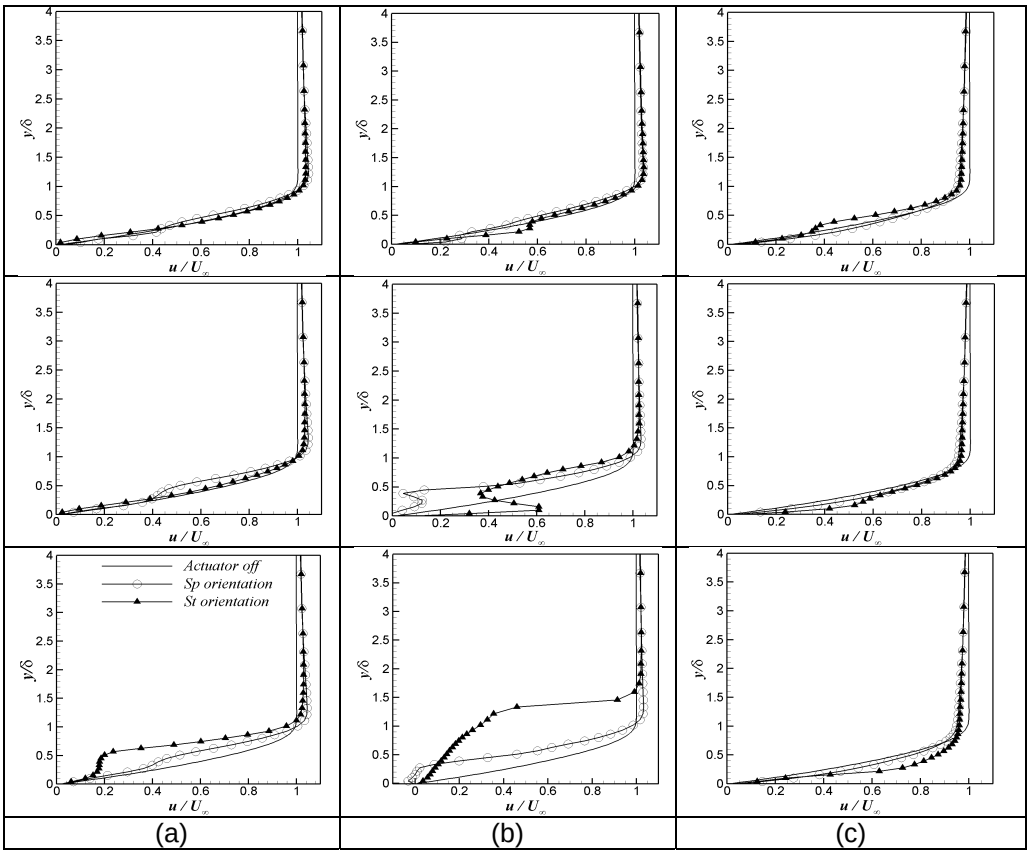

Figure 7. Instantaneous streamwise velocity at x/d=4 and three spanwise locations *z/d*=0 (bottom row), *z/d*=-1.5 (middle row) and *z/d*=-3.0 (top row) in three phases (a) $\phi = 90^\circ$, (b) $\phi = 180^\circ$, and (c) $\phi = 270^\circ$

Figure 7(c) shows the velocity profiles at $\phi = 270^\circ$ which is the maximum ingestion phase. It is clear that the velocity is almost unchanged for the spanwise oriented slot case within the boundary layer, whereas changing in the velocity for the streamwise oriented slot case at *z/d*=0 and *z/d*=-1.5 reveals that the effect of the jet is sustained for a longer time in this case than the spanwise oriented slot case.

3.1.2 Time-averaged flow field

To further quantify the differences between the two cases, we compare the time-averaged *u*-velocity and fluctuation kinetic energy (*FKE*) profiles at three locations (*x/d*=4, 10 and 22) along the centerline downstream of the synthetic jet in Figure 8. The fluctuations u' and v' are based off the baseline unexcited flow for both synthetic jet cases. It is clear that in all locations, the *u*-velocity immediately near the surface is greater in the streamwise oriented slot case than the other case, and the difference increases with the downstream distance. It is also observed that the flow penetration into the boundary layer in the streamwise oriented slot increases with the streamwise distance whereas no noticeable change in the velocity profile is obtained in the spanwise oriented slot case.

The second row in Figure 8 shows the mean fluctuation kinetic energy (*FKE*) non-dimensionalized by the square of free-stream velocity. At *x/d*=4, the strong streamwise vortices, produce large velocity fluctuations at the centerline in the streamwise oriented slot case with a peak which is three times greater than the spanwise oriented slot case. Further downstream, the fluctuation level in the streamwise oriented slot case changes quite significantly whereas that of the spanwise oriented slot case remains roughly the same. However, in all streamwise locations shown in Figure 8, the peak *FKE*

for the streamwise oriented case remains significantly larger than the peak *FKE* for the spanwise oriented slot case.

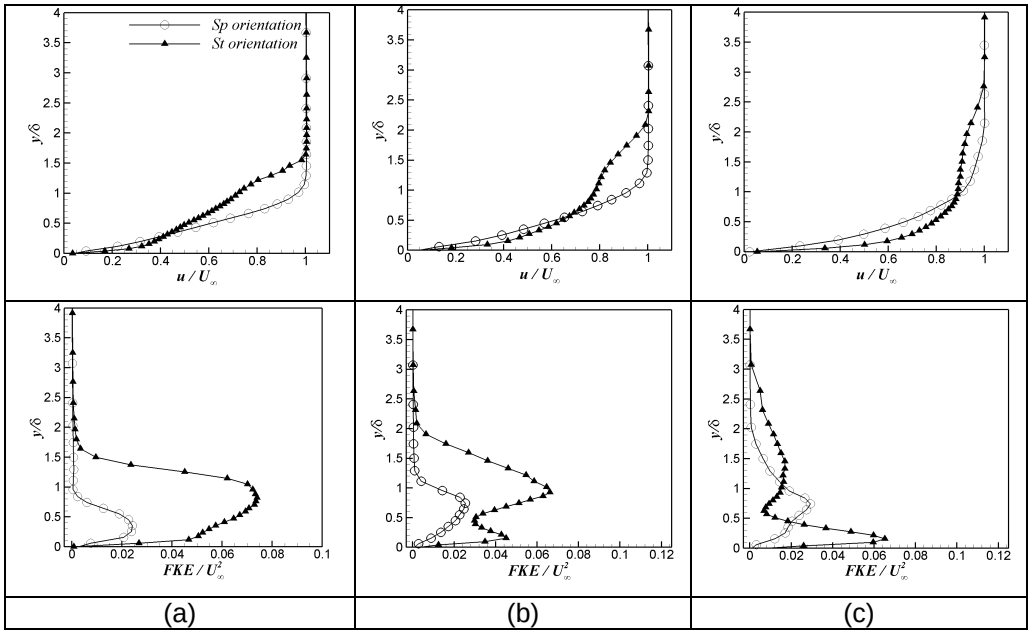

Figure 8. Time average *u*-velocity (first row) and fluctuation kinetic energy (second row) profiles on the the centerline at (a) *x/d*=4, (b) *x/d*=10, and (c) *x/d*=22

In order to gain further insight into the flow physics of these two jets in cross flow and clarify the mechanism that modifies the boundary layer, we examine the "sweeping" [44] motion associated with the vortex structures produced by the two cases by evaluating the conditional averages of $u'v'$. Note that a sweeping motion refers to the downward induced flow of higher momentum fluid into the boundary layer and is characterized by a positive value of u' and a negative value of v':

$$\overline{< u'v' >_S} = \frac{1}{T}\int_0^T < u'v' >_S dt \tag{4}$$

where subscripts "S" represent conditional averages for the sweep events. The first row of Figure 9 shows the iso-surface of the conditional average for the sweeping motion for both slot orientations. It is clear that the downwash of the flow mainly occurs in a limited region outboard of the slot in the spanwise oriented slot configuration. In contrast, in the streamwise oriented slot case, the sweep events are produced not only along the wall due to the legs of the hairpin vortices but also prodiced further downstream due to the heads of the hairpins.

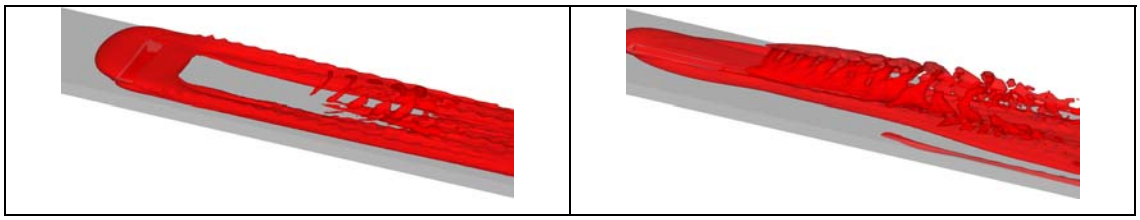

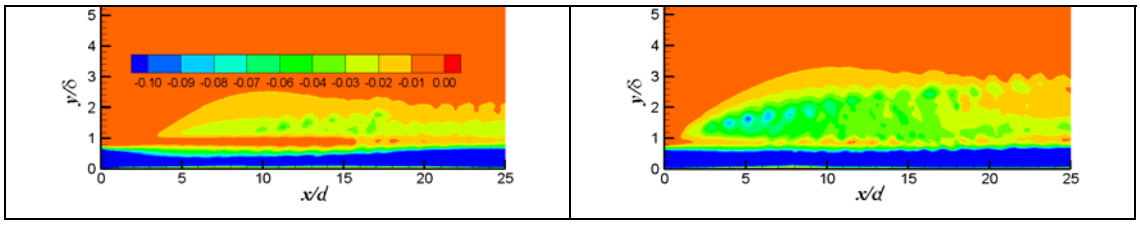

Figure 9. Iso-surface of "sweep" for the spanwise oriented (top left) and streamwise oriented slots (top right) and contours of spanwise average of this quantity for the spanwise oriented (bottom left) and streamwise oriented slots (bottom right)

A spanwise average of the conditional average provides a good estimate of the overall effect of an infinite periodic array of these synthetic jets on the momentum exchange between the outflow and the boundary layer. This quantity is plotted in the second row of Figure 9 for both slot configurations. For both cases, the large values of this quantity occur within the boundary layer. However, while the streamwise oriented slot produces a nearly even amount of downwash everywhere in the boundary layer, there is significant reduction in this quantity for the spanwise oriented slot between x/d = 5 and 17. There is also a region of downwash outside the boundary layer and this is associated with the "head" of the hairpin vortices. We note that while for the spanwise oriented slot, significant downwash of high momentum fluid outside the boundary layer occurs within the small regions which starts somewhere around 10d downstream of the slot, it occurs much closer (around 2d) in the streamwise oriented slot case. This would suggest that for the separation control, a spanwise oriented slot would have to be placed significantly upstream of the separation point to be effective.

The streamwise component of the wall shear stress is another parameter that characterizes the momentum in the innermost region of the boundary layer; a higher value of this quantity implies a higher resistance to the adverse pressure gradient and separation. The spanwise distribution of this parameter (τ_w) normalized by the baseline value (τ_{w_b}) at five different streamwise locations for both cases are plotted in Figure 10(a) and 10(b), respectively where the dashed lines denote the spanwise extent of the slots. For the spanwise oriented slot case, the maximum wall shear stress occurs near the slot edges at all streamwise locations. A secondary maximum is seen near the centerline for this case and this corresponds to the location where the hairpin structure is generated in the downstream region. The peak value also diminishes somewhat from x/d=2 to x/d=10 and becomes almost constant beyond that station in this case. In the streamwise oriented slot case, two maxima in wall stress are generated in the vicinity of the slot (x/d=2, 4) slot edges, and these eventually combine into a single peak along the centerline of the slot which increases along the x direction. No noticeable variation in this parameter is observed at x/d=18, and 22 in this case.

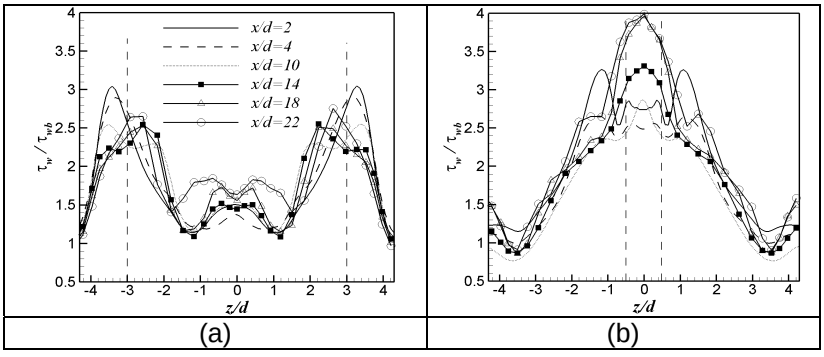

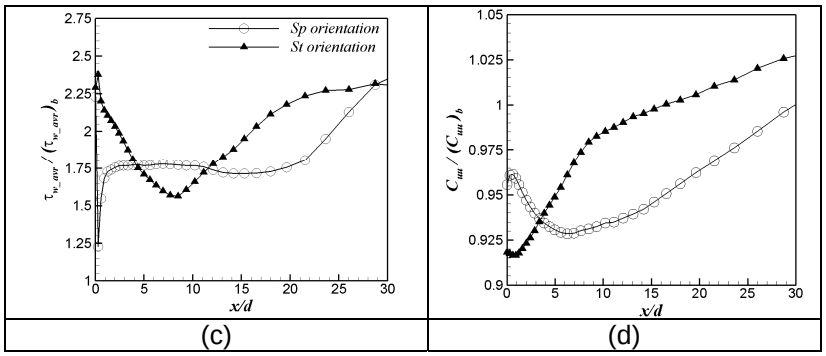

Figure 10. Spanwise distribution of the streamwise component of wall shear stress (τ_w) at different *x/d* for the (a) spanwise oriented slot, (b) streamwise oriented slot, (c) streamwise variation of span-averaged τ_w, and (d) streamwise variation of momentum flux for both orientations.

A key point to note is that beyond *x/d*=10, the peak as well as the spanwise average shown in Figure 10(c) of the wall shear stress is higher for the streamwise oriented slot case. This is consistent with the stronger sweep events associated with the hairpin vortex structures which bring high momentum outer fluid down into the boundary layer which is desirable for separation control. As pointed out by Jabbal & Zhong [14], persistence of the jet in the boundary layer is an important characteristic for the control effectiveness of a synthetic jet. This characteristic of the jet is also essential if the separation location of boundary layer is not possible to identify in advance or as Jabbal & Zhong [14] mentioned, implementation of synthetic jets in the vicinity of the mean separated flow is not doable. The plot of the average shear stress show that indeed the streamwise oriented slot case exhibits stronger persistence. However to more clearly quantify this property of the jet, we compare the streamwise variation of the time-averaged momentum flux estimated by

$$C_{uu} = \int_{-L_z/2}^{L_z/2} \int_0^{\delta} \overline{u}^2(x,y,z)dydz \tag{5}$$

for both slot orientations, where L_z is the spanwise length of the computational domain. It is observed that beyond about *x/d*=3, the streamwise oriented slot consistently generates a higher value of this flux than the spanwise oriented slot configuration. This comparison reveals that beyond *x/d*=8.0 the streamwise momentum flux in the streamwise oriented slot case becomes significantly higher than the other case and this difference is maintained for a long streamwise distance from the slot.

3.2 Jet Interaction with Separated Flow over a Hump

In this section, the characteristics of the separated flow over a wall mounted hump as well as the effect of the slot orientation on the separation control are investigated.

3.2.1 Baseline Separated Flow

Since no published data is available for the 3D flow over the hump at the current Reynolds number to validate current results, 2D simulations of this case have been carried out with the express purpose of validating against the 2D numerical simulation of Franck [38]. Figure 11(a) compares the time average of pressure coefficient over the hump of the current 2D and 3D simulations with the 2D simulations of Franck [38]. The reference pressure p_{ref} is obtained by enforcing $\overline{C}_p = 1$ at the stagnation point. With the exception of difference between the current 2D simulation and work of Franck [38] in the separation region, reasonable prediction is seen for this aerodynamic parameter. It should be noted that Franck [38] considered a compressible flow with a Mach number of 0.25 in their simulations and showed that increasing the Mach number from *M*=0.25 to 0.6 caused a significant delay in

reattachment of the boundary layer and displacement of secondary bubble. It is therefore possible that the difference between the two computed results could be due to the compressibility effects of the flow which are not included here.

As mentioned earlier, a grid dependency study for the 3D baseline case has been carried out by removing the slot-related grid refinement, and applying a finer grid in the separation region in the *x*-*y* plane (25% increase in the grid resolution of separated region in each direction which leads to nearly twice the number of grid points in this region) and a uniform grid in the *z* direction (the original grid is non-uniform in the *z* direction). Figure 11(b) shows the time-span averaged streamlines for both grids. There is a good agreement seen for the separation point and bubble size between the simulations obtained on the two grids, with a difference of the reattachment point location being only 6% of the bubble length.

The spanwise-average of the time-averaged pressure coefficient is also extracted for both grids given in Figure 11(a) and the favorable comparison indicates that the grid employed is sufficient for the current simulations. Acceleration of the boundary layer over the leading edge (concave section) of the hump causes a reduction in the pressure (favorable pressure gradient) with a suction peak at $x/c\approx0.42$. This is followed by pressure recovery (adverse pressure gradient) over the trailing edge (convex section) which leads to the separation of boundary layer at $x/c\approx0.59$. A large plateau region seen in the trailing-edge corresponds to the separation of boundary layer which eventually reattaches at $x/c\approx2.1$. Comparing current numerical results at $Re_c=1.5\times10^4$ with the experimental results of Seifert and Pack [23] at $Re_c=16\times10^6$ shows that while the pressure distribution is similar over the front side of the hump, differences in the minimum pressure (from -0.08 to 0.3), earlier separation of boundary layer (from $x/c\approx0.66$ to $x/c\approx0.59$) and a larger recirculation zone in the separation bubble region are observed in the current simulation due to the lower momentum of fluid.

Comparing the pressure distribution of the 3D baseline flow with that obtained from the 2D simulation (Figure 11(a)) we find that although the 3D flow behaves very similar to the 2D flow before the separation point with a same suction peak and separation location, the separated region is intrinsically 3D for this flow configuration with a larger recirculation bubble length than the 2D case. This suggest that a two dimensional modeling of this flow leads to an inaccurate prediction of governing flow physics and aerodynamic quantities over the hump.

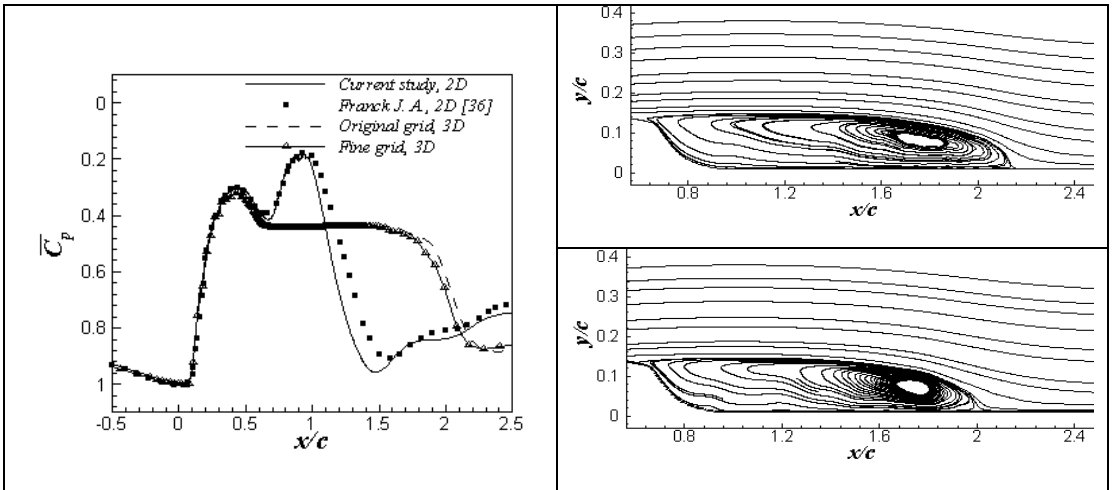

Figure 11. (a) Time-averaged pressure coefficient for the 2D and 3D simulations, (b) time-span average of the streamlines (first row is the original grid, second row is the fine grid)

In order to obtain the dominant frequency of the separation bubble for flow control purpose, the power spectrum of the cross-stream velocity are extracted at different locations in the recirculation region. Figure 12 shows a spanwise averaged power spectrum of the temporal variation of cross stream velocity at one *x*-*y* location in the separation bubble zone with the dominant peak at $F^+=1.87$, where

the dashed lines represent the inertial subrange ($k^{-5/3}$ line). The lack of a clear inertial subrange indicates that the separated zone is transitional at best. It needs to be mentioned that all of the probe points in the separation zone show the same dominant frequency and a similar trend.

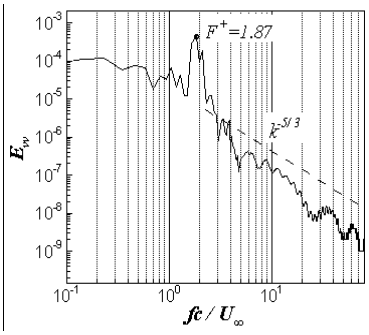

Figure 12. Span-averaged power spectrum of cross-stream velocity for the baseline flow

3.2.2 Control of Flow Separation

As mentioned before, the performance of the synthetic jet actuator for both configurations in separated flow is examined at three different jet to free-stream velocity ratios including $\overline{V_J}/U_\infty$=0.095, 0.254 and 0.445, where the forcing frequency is kept constant at dominant baseline frequency of F^+=1.87 for all jet amplitudes. The nominal case in this study is considered as a synthetic jet with a jet to free-stream velocity of $\overline{V_J}/U_\infty$=0.254 and a forcing frequency of F^+=1.87 in both slot configurations.

Figure 13 shows the instantaneous iso-surface of swirl strength with a non-dimensional magnitude of $650Qd/U_\infty$ in the vicinity of both slot orientations for the nominal case. The two snapshots shown in this figure, which are colored by the contours of the cross stream velocity ($v/\overline{V_J}$), represent end of the expulsion phase ($\phi = 180^\circ$) and ingestion phase ($\phi = 270^\circ$) of excitation. Similar to what we have found in the case of attached boundary layer over the flat plate, the dominant feature for the spanwsie oriented slot case during the expulsion phase (Figure 13 a(i)) is the formation of spanwise structures in the vicinity of the slot exit along the span, which are convected downstream by the cross-stream flow. In contrast, a pair of counter rotating streamwise vorticites along the long edges of streamwise oriented slot is observed in Figure 13 b(i) which forms the legs of a large hairpin vortex.

Another feature which was also seen in the case of attached flow, is the formation of two small streamwise oriented vortices along the spanwise ends of the slot, which causes a spanwise contraction of the vortical structures that emanate from the slot. These streamwise structures, which attach to the spanwise vortices are stretched along the streamwise direction by the cross-stream flow until the end of expulsion phase (Figure 13 a(i)). The stretching phenomenon also occurs for the legs of the hairpin structure in the streamwise oriented slot case and is not limited to the expulsion phase only for this case.

While the small streamwise oriented structures detach from the end-span edges of the spanwise oriented slot and are convected downstream together with the primary spanwise vortices during the ingestion phase (Figure 13 a(ii)), the two legs of hairpin structures still attach to the slot and stretched along the streamwise direction in the streamwise oriented slot case (Figure 13 b(ii)); this can provide a beneficial effect on delaying the onset of boundary layer separation even during the ingestion phase.

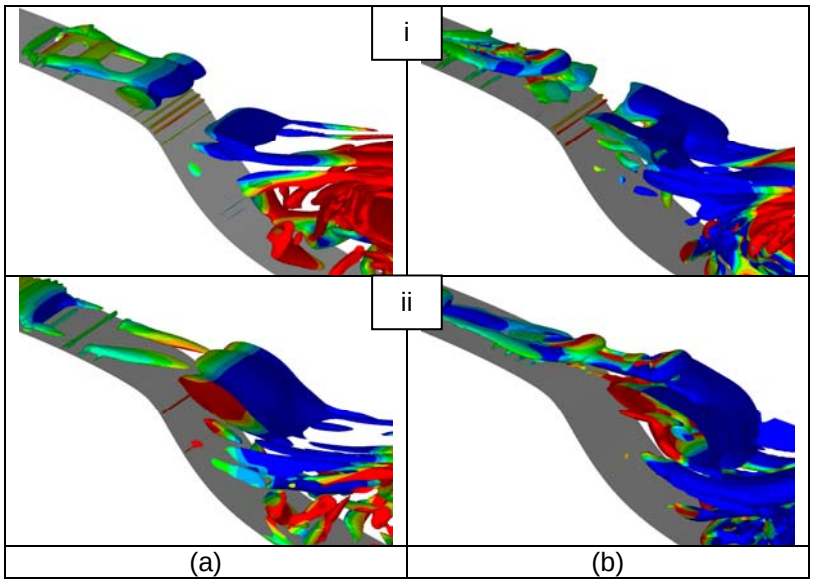

Figure 13. Instantaneous iso-surface of the swirl strength colored by the cross-stream velocity for the (a) spanwise oriented and (b) streamwise oriented slots at: (i) $\phi = 180^{\circ}$ (end of expulsion phase), (ii) $\phi = 270^{\circ}$ (end of ingestion phase)

Figure 14(a) shows the span-averaged locus of the zero *u*-velocity in the separation zone for the nominal case which is non-dimensionalized by the height of the hump (*H*). This curve, which represents the height of reverse flow layer is obtained by finding the vertical distance between the hump wall and the location in the separation bubble where the span-time-averaged *u*-velocity changes its sign from negative to positive. The plot shows that the streamwise oriented slot case introduces a smaller reverse flow height in comparison with the other slot configuration case with a maximum difference of $\Delta y_0/H$= 0.31 at x/c=1.29. While no significant difference is seen between the two cases for the location of the separation point, the streamwise orientation causes earlier reattachment of boundary layer and consequently, a shorter bubble length (L_{sep}/c=0.651 in the streamwise oriented slot case versus 0.727 in the spanwise oriented slot case). The area under the curve (A_{sep}) which combines the height and length of bubble in the reverse flow zone is another measure that can be used to study the effect of synthetic jet on the aerodynamic quantities such as drag or lift. This parameter, which is non-dimensionalized by the chord length and the maximum height of the hump, is also smaller in the streamwise oriented slot case (A_{sep}/cH =0.16) than the spanwise oriented slot case (A_{sep}/cH=0.2).

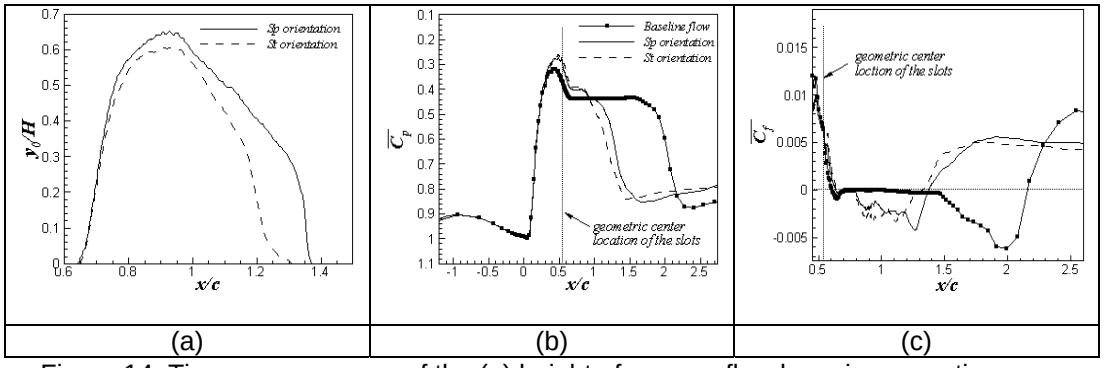

Figure 14. Time-span average of the (a) height of reverse flow layer in separation zone above the wall, (b) pressure coefficient, and (c) wall shear stress for nominal controlled case

The time-span averaged pressure coefficient of the controlled flow (nominal case) over the hump is compared with the baseline uncontrolled flow in Figure 14(b) and reveals a significantly smaller plateau and consequently, a dramatic reduction in the length of the bubble caused by the synthetic jet in both slot orientations. An earlier pressure recovery in the separation zone and consequently, a higher pressure in this region for the streamwise oriented slot case would produce a lower pressure drag for an airfoil configuration.

The skin friction coefficient is another non-dimensional parameter that can be used to study the flow control effectiveness. The time-span average of this coefficient is seen in Figure 14(c) for the baseline as well as controlled flow cases in the nominal operational condition. As observed in this graph, there is a large region of nearly zero skin-friction for the uncontrolled case that extends from downstream of the separation point to about x/c=1.5. This is a characteristic of a weak reverse flow in the lee side of the hump. Downstream of x/c=1.5 there is a stronger backflow and this produces significant negative values of the skin friction coefficient with the reattachment occurring at around x/c=2.15.

In contrast to this case, both the controlled cases show a slight delay in separation. Furthermore the entire region of backflow is significantly reduced for both these cases; the region of nearly zero shear stress immediately downstream of the separation point now only extends to about x/c=0.8 and the reattachment point have moved upstream to about x/c=1.3. We note that the reattachment point for the streamwise oriented slot is upstream of the other case and this is consistent with the superior performance of the streamwise oriented jet that is noted based on the other measured discussed earlier.

The effect of slot orientation on the separation line along the span at two jet to free-stream velocity ratios of $\overline{V}_J / U_\infty$ =0.254 and 0.445 is seen in Figure 15. Formation of strong coherent structures in the spanwise oriented slot case causes a blockage of flow and an earlier separation of the boundary layer in the mid-span region. In contrast, in the outer spanwise regions of the slot this jet blockage is minimal and the emanation of small streamwise oriented vortices from the spanwise ends of the slot leads to a delay in separation. As expected, the effect of the jet blockage on the separation point in the mid-span is intensified by increasing the jet amplitude. In contrast, the largest delay in separation of the boundary layer occurs on the centerline in the streamwise oriented slot case. Increasing the jet amplitude enhances the delay in the boundary layer separation due to the generation of a stronger hairpin vortex which can penetrate deeper into the higher momentum fluid and sweep it down to the surface. A quicker spread of the jet via a pair of counter rotating streamwise vortices that are the legs of hairpin structure is also observed in this case. Span-average of separation location shows that the nominal flow control case causes 5% and 6% of chord length delay in the separation for the spanwise and streamwise orientated slot cases, respectively.

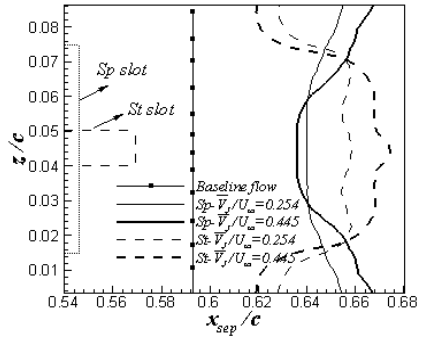

Figure 15. Time-averaged spanwise distribution of the separation point x_{sep}/c for the baseline flow and controlled cases at two jet velocity amplitudes

A comparison of the time-span-averaged pressure coefficient at different jet amplitudes for the streamwise oriented slot case is shown in Figure 16(a). As it is clear, the synthetic jet is able to modify this coefficient for all forcing amplitudes. Increasing the jet amplitude leads to an increase in the

suction peak before the separation of the boundary layer. While a change of $\overline{V}_J / U_\infty$ from 0.095 to 0.254 enhances the pressure recovery in the recirculation region, further increase of this operational parameter does not significantly change the pressure distribution over the hump in the streamwise oriented slot configuration. The effect of the jet excitation frequency on the time-span averaged pressure coefficient for the spanwise and streamwise oriented slot cases is also presented in Figure 16(b) and (c), respectively. It bears reminding that the most energetic frequency in the baseline, uncontrolled flow is 1.87. A delay in the pressure recovery within the separation zone with increasing excitation frequency is observed in both slot orientation cases.

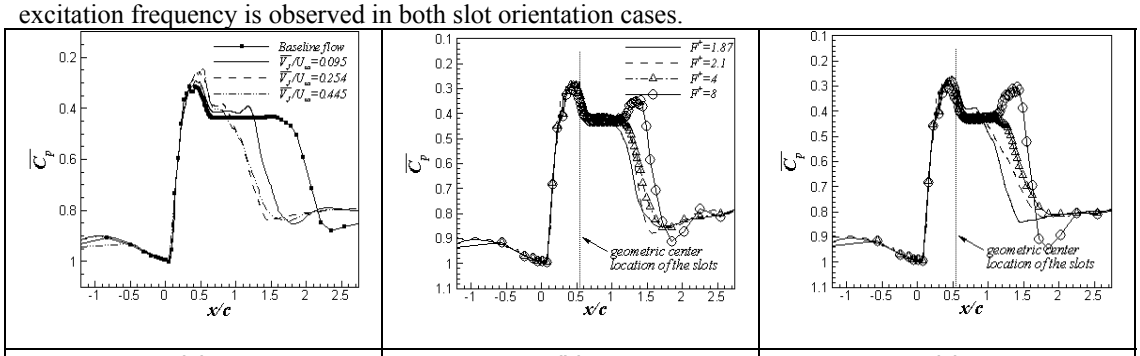

(a) (b) (c)

Figure 16. Spanwise average of the mean pressure coefficient (a) at different forcing amplitudes in the streamwise orientated slot case, and at different forcing frequencies in the (b) spanwise oriented slot case, (c) streamwise oriented slot case

Table 1 summarizes the data regarding the time-span average of the locations of the separation and reattachment points, separation bubble length and percentage difference of the separation bubble length for both slot configuration cases at different forcing amplitudes and frequencies. It is clear that for all jet amplitudes with the same forcing frequencies, the separation of boundary layer is delayed further in the streamwise oriented slot configuration than the spanwise oriented slot case. Furthermore, earlier reattachment is obtained in the former case which implies a shorter averaged bubble length for this slot orientation. Nonlinear effects of the jet amplitude on the separation bubble are also observed from these results (See Figure 17); the table clearly shows that the streamwise oriented slot with $\overline{V}_J / U_\infty$=0.254 provides more effective separation reduction than the spanwise oriented slot with $\overline{V}_J / U_\infty$=0.445, which has nearly twice the momentum flux. The last column in this table shows the difference between the bubble lengths obtained for both slot configuration cases ($\Delta L_{sep}/c=(L_{sep,sp}-L_{sep,st})/c$) which has the highest value of 7.6% in the nominal operational condition.

A comparison of the performance of the actuator for both slot orientations at a slightly higher frequency (F^+ =2.1) than the dominant frequency of the baseline flow (F^+=1.87) indicates that the streamwise oriented slot configuration is more effective in delaying separation, accelerating reattachment and reducing the bubble length at this frequency. While forcing the flow at almost twice the dominant frequency (F^+=4) of the baseline flow leads to a longer delay in separation of boundary layer in the streamwise oriented slot case than the spanwise oriented slot configuration, it also causes the reattachment of the boundary layer to occur further downstream. As a result of this, the bubble length in the streamwise oriented slot case is larger than the other configuration, which is the only exception in this range of study.

Table 1. Summary of the separation bubble location and its length at different jet amplitudes and frequencies

			Spanwise orientation			**Streamwise orientation**			
$\overline{V}_J / U_\infty$	C_μ	F^+	x_{sep}/c	x_{re}/c	L_{sep}/c	x_{sep}/c	x_{re}/c	L_{sep}/c	$\Delta L_{sep}/c$ (%)
0.095	**9×10^{-5}**	**1.87**	0.634	1.540	0.906	0.638	1.510	0.872	3.4

0.254	**6×10^{-4}**	**1.87**	0.644	1.371	0.727	0.65	1.301	0.651	7.6
0.445	**2×10^{-3}**	**1.87**	0.648	1.317	0.669	0.654	1.300	0.646	2.3
0.254	**6×10^{-4}**	**2.1**	0.641	1.459	0.818	0.647	1.445	0.798	2.0
0.254	**6×10^{-4}**	**4**	0.639	1.550	0.911	0.641	1.580	0.939	-2.8
0.254	**6×10^{-4}**	**8**	0.632	1.686	1.054	0.630	1.655	1.025	2.9

A summary of slot orientation effect on the time averaged quantities at different forcing amplitudes and frequencies for the flow over the wall-mounted hump is shown in Figure 17. The key observations in this study are as follows:

1. For almost all operational conditions in the range of study (except the high forcing frequency where the actuator effectiveness is the lowest), the streamwise oriented slot is more effective in delaying separation and accelerating the reattachment of the boundary layer. Consequently, both the length and area of the separation bubble are reduced to a higher degree for the streamwise oriented slot.

2. The current results confirm the conclusion of the study of the jet orientation in an attached boundary layer presented in the first part of the paper, that the hairpin vortices generated by the streamwise oriented jet are more effective in transporting high momentum fluid into the separating boundary layer.

3. The overall difference between the two slot orientation cases is relatively modest (maximum different in mean separation bubble length is 7.6%) but this may be due to the low Reynolds number of the current study as well as the fact that the separation studied here is quite robust due to the large adverse pressure gradient. Notwithstanding the modest difference here, there is little doubt that from the viewpoint of effective SJ based flow control, the streamwise oriented slots should be preferred over the spanwise oriented slots. This seems to contradict the simplistic notion intrinsic to many past studies that the spanwise oriented slots are better for flow control.

4. For the range studied in the current simulations, it is observed that increasing the jet amplitude monotonically improves the actuator performance for both slot orientations.

5. The most effective separation control is found for the lowest forcing frequency which in the current study, matches the most energetic frequency of the baseline (uncontrolled separated flow). This result is consistent with many past studies that have employed two-dimensional or nearly two-dimensional slots [45, 46]. Thus the underlying flow physics associated with separation reduction, i.e. vortices induce mixing that brings in high momentum outer fluid into the boundary layer, is quite robust even in the face of significant changes such as in the slot orientation.

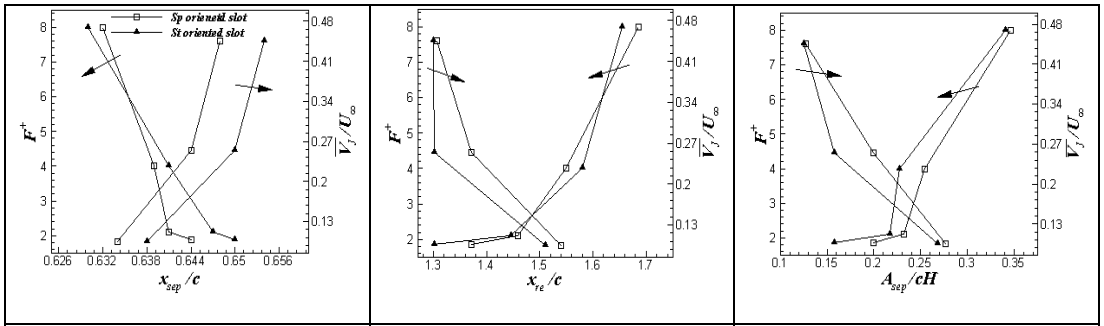

(a) (b) (c)

Figure 17. Effect of jet velocity and forcing frequency on the time-span average of (a) separation point, (b) reattachment point, and (c) area of reversed flow layer in separation bubble

4. CONCLUSIONS

Numerical simulations have been carried out to study the interaction of a synthetic jet with a rectangular slot with an attached laminar boundary layer as well as a separated flow. The primary goal

of this study was to explore the effect of slot orientation for a jet with a relatively large aspect-ratio (six in this case) on the boundary layer and the associated implications for separation control. Two slot orientations were chosen in this study: in one, the long axis of the slot was oriented in the spanwise direction and in the other, in the streamwise direction. We have found that the key difference in the two configurations is due to the vortical structures that are formed in the two cases; in the spanwise oriented slot case, the vorticity from the slot is primarily oriented in the spanwise direction but the clockwise component of this vorticity is severely diminished by its interaction with the counterclockwise vorticity in the boundary layer. For the streamwise oriented slot case, the dominant feature is a pair of counter-rotating streamwise vortices which constitute the legs of a hairpin vortex. The hairpin is found to amplify in strength due to the stretching action of the downstream flow and also spawn a sequence of hairpins upstream of the main structure.

The overall effect of this difference in vortex topology and evolution is that the jet from the streamwise oriented slot penetrates further outwards into the boundary layer and also produces a more substantial downwash ("sweep") of high momentum fluid into the boundary layer. This sweeping motion leads to substantial enhancement of streamwise momentum in the boundary layer and this enhances the ability of the boundary layer to better withstand an adverse pressure gradient. We also find that the improved momentum transport characteristics of the perturbed boundary layer establish more rapidly (closer to the jet exit) and persist for a longer streamwise distance from the slot for the streamwise oriented slot case. This would also indicate that the streamwise oriented slot configurations is more effective for separation control, especially in cases where the point of separation is not known a-priori.

The difference in vortical structures between two slot configuration cases was also seen in the case of a separated flow over a wall-mounted hump. This difference was enhanced by increasing in jet amplitude which introduced different behavior by the synthetic jet on the flow before the separation point and consequently on the separation bubble. A higher vertical penetration of the jet in the streamwise oriented slot case due to the mutual induction of streamwise vortices enhances downwash of high momentum outer fluid down into the boundary layer and delays in boundary layer separation for all jet amplitudes and most jet frequencies studied here. A smaller area of reversed flow in the separation zone, an earlier pressure recovery and as a result, an earlier reattachment of boundary layer were also observed in the case of the streamwise oriented slot. Among all forcing frequencies applied for flow separation control, it was found that the most effective forcing frequency was the one that matched the most energetic frequency of the baseline flow. Jet orientation is therefore a key feature in synthetic jet actuators and should be considered carefully in any separation control application.

ACKNOWLEDGMENTS

The work was supported by AFOSR under Grant FA9550-09-1-0257, monitored by Dr. Douglas Smith. This work was also supported in part by the U.S. National Science Foundation, grant NSF-OCI-108849 which provided computational resources for some of the simulations. Discussions with Dr. Louis Cattafesta of the University of Florida are gratefully acknowledged.

REFERENCES

[1] Prandtl, L., "Über Flüssigkeitsbewegung bei sehr kleiner Reibung," *Proceedings of the Third International Mathematicians Congress*, Heidelberg, Germany, 1904, pp. 484-491.

[2] Gad-El-Hak, M., *Flow Control: Passive, Active, and Reactive Flow Management*, Cambridge University Press, London, UK, 2000, Chaps 1.

[3] Trávníček, Z., and Tesař, V., "Annular Synthetic Jet Used for Impinging Flow Mass–Transfer," *International Journal of Heat and Mass Transfer*, Vol. 46, No. 17, 2003, pp. 3291-3297.

[4] Mahalingam, R., and Glezer, A., "Design and Thermal Characteristics of a Synthetic Jet Ejector Heat Sink," *Journal of Electronic Packaging*, Vol. 127, No. 2, 2005, pp. 172-177.

[5] Smith, B. L., and Glezer, A., "Jet Vectoring Using Synthetic Jets," *Journal of Fluid Mechanics*, Vol. 458, 2002, pp. 1–34.

[6] Pack, L. G., and Seifert, A., "Periodic Excitation for Jet Vectoring and Enhanced Spreading," *AIAA Journal*, Vol. 38, No. 3, 2001, pp. 486-495.

[7] Wang, H., and Menon, S. "Fuel-Air Mixing Enhancement by Synthetic Microjets," *AIAA Journal*, Vol. 39, No. 12, 2001, pp. 2308-2319.

[8] Chen, Y., Liang, S., Aung, K., Glezer, A., and Jagoda, J., "Enhanced Mixing in a Simulated Combustor Using Synthetic Jet Actuators," *AIAA paper 99-0449*, 1999.

[9] Maldonado, V., Farnsworth, J., Gressick, W., and Amitay, M., "Active Control of Flow Separation and Structural Vibrations of Wind Turbine Blades," *Journal of Wind Energy*, Vol. 13, Issue 2-3, 2009, pp. 221 – 237.

[10] Crook, A. and Wood, N. J., "Measurements and visualizations of synthetic jets," *AIAA Paper 2001-0145*, 2001.

[11] Mittal, R., Rampunggoon, R., and Udaykumar, H. S.,"Interaction of a synthetic jet with a flat plate boundary layer," *AIAA Paper 2001-2773*, 2001.

[12] Mittal R. and Rampunggoon, P., "On the virtual aero shaping effect of synthetic jets," *Brief Communications, Physics of Fluids*, Vol. 14, No. 4, 2002.

[13] Zhong, S., Mittet, F. and Wood, N. J., "The behavior of circular synthetic jets in a laminar boundary layer," *Aeronautical Journal*, Vol. 109, No. 461, 2005.

[14] Jabbal, M. and Zhong, S., "Particle image velocimetry measurements of the interaction of synthetic jets with a zero-pressure gradient laminar boundary layer," *Physics of Fluids*, Vol. **22**, Issue 6, 2010.

[15] Schaeffler, N. W. and Jenkins, L. N., "Isolated synthetic jet in crossflow: experimental protocols for a validation dataset," *AIAA Journal*, Vol. 44, No. 12, 2006.

[16] Gorden, M. and Soria, J., "PIV measurements of a zero-net-mass-flux jet in cross flow," *Experiments in Fluids*, Vol. **33**, No. 6, 2002.

[17] Wu, D. K. L. and Leschziner, M. A., "Large-eddy simulations of circular synthetic jets in quiescent surroundings and in turbulent cross flow," *International Journal of Heat and Fluid Flow*, Vol. **30**, No. 3, 2009.

[18] Dandois, J., Garnier, E. and Sagaut, P., "Unsteady simulation of a synthetic jet in a cross flow," *AIAA Journal*, Vol. 44, No. 2, 2006.

[19] Zhou, J. and Zhong, S., "Numerical simulation of the interaction of a circular synthetic jet with a boundary layer," *Computer and Fluids*, Vol. **38**, No. 2, 2009.

[20] Vasile, J., Elimelech, Y., Farnsworth, J., Amitay, M. and Jansen, K. E., "Interaction of a finite-span synthetic-jet and cross-flow over a swept wing," *AIAA paper* 2010-4584, 2010.

[21] Smith, D. R., "Interaction of a synthetic jet with a crossflow boundary layer," *AIAA Journal*, Vol. 40, No. 1, 2002.

[22] Milanovic, I. M. and Zaman, K. B. M. Q., "Fluid dynamics of highly pitched and yawed jets in cross flow," *AIAA Journal*, Vol. 42, No. 5, 2004.

[23] Seifert, A., and Pack, L., "Active Flow Separation Control on Wall-Mounted Hump at High Reynolds Numbers," *AIAA Journal*, Vol. 40, No. 7, 2002, pp. 1363–1372.

[24] Rumsey, C. L., Gatski, T. B., Sellers, W. L., Vatsa, V. N., and Viken, S. A., "SumMary of the 2004 Computational Fluid Dynamics Validation Workshop on Synthetic Jets," *AIAA Journal*, Vol. 44, No. 2, 2006, pp. 194–207.

[25] You, D., Wang, M., and Moin, P., "Large-Eddy Simulation of Flow over a Wall-Mounted Hump with Separation Control," *AIAA Journal*, Vol. 44, No. 11, 2006, pp. 2571–2577.

[26] Saric, S., Jakirlic, S., Djugum, A., and Tropea, C., "Computational Analysis of Locally Forced Flow over a Wall-Mounted Hump at High-Re Number," *International Journal of Heat and Fluid Flow*, Vol. 27, No. 4, 2006, pp. 707–720.

[27] Rumsey, C. L.," Reynolds-Averaged Navier-Stokes Analysis of Zero Efflux Flow Control over a Hump Model", *Journal of aircraft*, 2007, Vol.44, No.2, pp. 444-452.

[28] Bettini, C., and Cravero, C., "Computational Analysis of Flow Separation Control for the Flow over a Wall-Mounted Hump Using a Synthetic Jet ", *AIAA paper 2007-516*, 2007.

[29] Franck, J. A., and Colonius, T., "Compressible Large-Eddy Simulation of Separation Control on a Wall-Mounted Hump," *AIAA Journal*, Vol.48, No. 6, 2010, 1098-1107.

[30] Aram, E., Mittal, R. and Cattafesta, L. N. , "Simple representations of Zero-Net Mass-Flux jets in Grazing flow for flow-control simulations," *International Journal of Flow Control*, Vol. **2**, No. 2, 2010.

[31] Raju, R., Aram, E., Mittal, R. and Cattafesta, L. N., "Simple models of Zero-Net Mass-Flux jets flow control simulations," *International Journal of Flow Control*, Vol. 1, No. 3, 2009.

[32] Ravi, B. R. , Mittal, R. and Najjar, F. M., "Study of three-dimensional synthetic jet flowfields using direct numerical simulation," *AIAA Paper* 2004-0091, 2004.

[33] Ravi, B. R. and Mittal, R., "Numerical study of large aspect-ratio synthetic jets," *AIAA Paper* 2006-0315, 2006.

[34] Holman, R. Utturkar, Y., Mittal, R., Smith, B. L. and Cattafesta, L., "Formation criterion for synthetic jets," *AIAA Journal*, Vol. 43, No. 10, 2005.

[35] Mittal, R. Dong, H., Bozkurttas, M., Najjar, F., Vargas, A. and Loebbecke, A., "A versatile immersed boundary method for incompressible flows with complex boundaries," *Journal of Computational Physics*, Vol. 227, No. 11, 2008.

[36] Aram, S., "A Computational study of synthetic-jet based separation control," PhD Thesis, Department of Mechanical Engineering, The Johns Hopkins University, Baltimore, MD, 2011.

[37] Schlichting, H. and Gersten, K., "Boundary layer theory," Springer, 2000, ISBN 3540662707.

[38] Franck, J. A., "Large-eddy simulation of flow separation and control on a wall-mounted hump," PhD Thesis, Mechanical Engineering, California Institute of Technology, Pasadena, CA, 2009.

[39] Vreman, A., "An Eddy Viscosity Subgrid-scale Model for Turbulent Shear Flow: Algebraic Theory and applications," *Physics of Fluids*, Vol. 16, pp. 3670–3680, 2004.

[40] Ramakrishnan, S., Zheng, L., Mittal, R., Najjar, F., Lauder, G. V. and Hedrick, T. L., "Large eddy simulation of flows with complex moving boundaries: application to flying and swimming in animals," *AIAA paper* 2009-3976, 2009.

[41] Chong, M. S., Perry, A. E. and Cantwell, B. J., "A general classification of three-dimensional flow field," *Physics of Fluids*, Vol. 2, No. 5, 1990.

[42] Acarlar, M. S. and Smith, C. R., "A study of hairpin vortices in a laminar boundary layer. Part 2. Hairpin vortices generated by fluid injection," *Journal of Fluid Mechanics*, Vol. 175, 1987.

[43] Erosy, S. and Walker, J. D. A., "Viscous flow induced by counter-rotating vortices," *Physics of Fluids*, Vol. 28**,** 1985.

[44] Wallace, J. M ., Eckelmann, H. and Brodkey, R. S., "The wall region turbulent shear flow," *Journal of Fluid Mechanics*, Vol. 54, 1972.

[45] Kotapati, R., Mittal, R., Marxen, O., Ham, F., You, D., and Cattafesta, L. N.,"Nonlinear Dynamics and Synthetic-Jet-Based Control of a Canonical Separated Flow," *Journal of Fluid Mechanics* 654, 2010.

[46] Aram, E., Mittal, R., Gri n, J., and Cattafesta, L., "Towards E ective ZNMF Jet Based Control of a Canonical Separated Flow," *AIAA Paper* 2010-4705, 2010.